Performance Analysis of Single-Phase Space Thermal Radiators and Optimization Through Taguchi-Neuro-Genetic Approach

P. B. Chiranjeevi
Deputy Project Director
Human Space Flight Centre,
Indian Space Research Organization,
Bengaluru 560094, Karnataka, India
e-mail: chiran-hsfc@isro.gov.in

V. Ashok
Deputy Director
Vikram Sarabhai Space Centre,
Indian Space Research Organization,
Trivandrum 695586, Kerala, India
e-mail: v_ashok@vssc.gov.in

K. Srinivasan[1]
Professor
Department of Mechanical Engineering,
Indian Institute of Technology Madras,
Chennai 600036, Tamil Nadu, India
e-mail: ksri@iitm.ac.in

T. Sundararajan
Professor
Department of Mechanical Engineering,
Indian Institute of Technology Madras,
Chennai 600036, Tamil Nadu, India
e-mail: tsundar@iitm.ac.in

In the thermal management of spacecraft, space thermal radiators play a vital role as heat sinks. A serial radiator with proven advantages in ground applications is proposed and analyzed for space applications. From the performance analysis, specific heat rejection (SHR) of serial radiator is found to be higher than parallel radiator by 80% for maximum diameter of the tube, 47% for maximum thickness of the fin, and 75% for maximum pitch of the tubes under consideration. Also, serial radiator requires four times higher pumping power than parallel radiator with geometric parameters and a maximum mass flowrate under consideration. In serial radiators, the cross conduction between the fins has a significant effect on its thermal performance. Thus, conjugate heat transfer simulations and optimization operations are to be performed iteratively to optimize the serial radiator, which is computationally costly. To reduce the computational time, artificial neural network (ANN) is trained using conjugate heat transfer simulations data and combined with the genetic algorithm (GA) to perform optimization. Taguchi's orthogonal arrays provided the partial fraction of conjugate heat transfer simulations set to train the ANN. Taguchi-Neuro-Genetic approach, a process that combines the features of three powerful techniques in different optimization phases, is used to optimize both parallel and serial radiators. The optimization aims to obtain a configuration that provides the lowest mass and lowest pumping power requirement for given heat rejection. Optimization results show that the conventional parallel radiator is about 20% heavier and requires about 35% more pumping power than the proposed serial radiator. [DOI: 10.1115/1.4052897]

Keywords: conjugate heat transfer analysis, design of experiments, Taguchi's orthogonal arrays, neuro-genetic optimization, multi-parametric optimization, extended surfaces/fins, heat exchangers, heat pipes, heat transfer enhancement

1 Introduction

Ever since USSR launched Sputnik in 1957, humans' urge to explore space increasing day by day. With an increase in the number of human space flights, there is a need to develop new technologies and optimize existing technologies. In a typical human space flight, the thermal control system (TCS), which is a subsystem of the Environmental Control and Life Support System (ECLSS), plays a vital role in maintaining the comfort cabin temperature for the crew and also in maintaining the electronic equipment within their operating temperature range. Heat sinks in TCS are usually the radiators, either body-mounted or deployed, which collect the heat from the coolant passing through the radiator tubes and reject it to deep space as electromagnetic radiation.

Figure 1 schematically represents the simplified hydro-pneumatic circuit of the TCS. The air-liquid heat exchanger housed inside the cabin collects the heat dissipated in cabin air and transfers it to the primary coolant passing through TCS. Internal habitat loop (IHL) consists of an air-liquid heat exchanger, electronics, interface heat exchanger, and the mechanically pumped fluid loop (MPFL), which includes pumps, solenoid valves, check valves, and flow proportioning valves. In the interface heat exchanger, heat is transferred from the primary coolant to a secondary coolant of TCS. The secondary coolant is passed through the radiators using the MPFL system to reject the heat to deep space, and this loop is called the external radiator loop (ERL). This study aims at analyzing the performance of radiators of the TCS in ERL.

From the early years of the space age to the recent past, researchers have investigated the performance of heat pipe radiators and optimized the design parameters [1]. With increasing power requirements for the recent missions, better heat removal strategies with MPFL systems are required. MPFL systems, in general, are used for massive satellites with higher heat dissipation rates. Afshari et al. [2] performed the optimization of tube pitch and length for a fixed pipe diameter of MPFL parallel radiators using a genetic algorithm (GA). The literature on the radiator applications on the ground for providing thermal comfort to living spaces was reviewed. Salem et al. [3] studied the effect of Aluminum and Copper nanoparticles enriched fluid passing through the serial radiators for ground applications. Võsa et al. [4] experimentally analyzed the heat rejection efficiency of parallel and serial radiator configurations. The authors concluded that the emission efficiency of serial radiator configuration is higher than that of parallel radiator configuration. Considering the higher emission efficiency of serial radiators, the present work proposes and studies serial radiators for space applications.

Mass optimization of the MPFL parallel radiator was undertaken by Kumar Rai et al. [5] through a semi-analytical approach. Several optimization tools exist for designing radiators. Numerous authors reported using a GA, a powerful tool for optimizing nonlinear, discontinuous, and nondifferentiable objective functions for optimizing various thermal systems [6,7]. Dias and Milanez [8] brought out the capabilities of GA through a comparative study with work reported by da Silva et al. [9], where an extensive search optimization technique was used for the same problem of heat source

[1]Corresponding author.

Manuscript received April 30, 2021; final manuscript received October 27, 2021; published online November 18, 2021. Assoc. Editor: Cheng-Xian Lin.

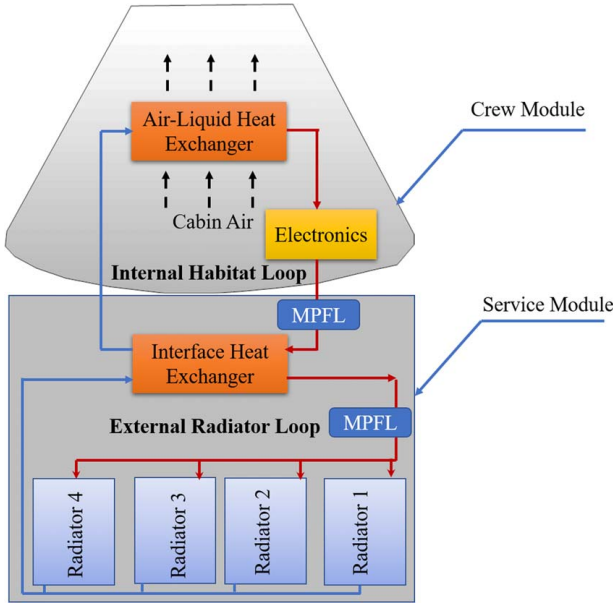

Fig. 1 Schematic of a hydro-pneumatic circuit of a thermal control system in a typical human space flight with parallel radiators

location optimization on a vertical wall with natural convection heat transfer. The authors reported that the number of simulations performed by GA to obtain accurate results is only about 2% of those required in extensive search, thus, largely reducing the computational time. Thus, GA is selected as a tool for optimizing the parallel and serial radiator configurations.

The thermal performance of parallel radiators can be mathematically modeled through analytical expressions, making them amenable for direct optimization. Whereas for serial radiators, where the cross conduction between the fins plays a vital role, the thermal performance can only be accurately estimated through conjugate heat transfer simulations. Optimization of serial radiators requires the interconnection of conjugate heat transfer simulations with GA. It is an iterative process in which the genetic algorithm predicts the new population, for which conjugate heat transfer analysis is to be carried out to provide fitness values to each iteration population. Interconnection of conjugate heat transfer simulations with the genetic algorithm is computationally costly. The artificial neural network (ANN), which is trained using the conjugate heat transfer simulation data, estimates the output parameters for a given set of input variables. Leong et al. [10] brought out the capabilities of ANN to predict the thermal performance of plastic-ball grid array. The authors showed that ANN predicts the junction temperature with 21 times better accuracy and the thermal resistance with 69 times better accuracy than multiple linear regression. Asok et al. [11] utilized ANN to relate the input parameters of static labyrinth seals with output parameters. The authors trained ANN using computational fluid dynamics data, and the trained ANN was used to predict the vortex loss coefficient and optimize the performance of square cavity labyrinth seals. Vortex generator for heat transfer enhancement in a plate-fin channel is optimized by Khan and Li [12] by combining the Bayesian-regularized artificial neural network, trained by computational fluid dynamics data and multi-objective optimization algorithm. Compared with the direct interconnection of conjugate heat transfer simulations with GA, trained ANN and GA coupling is computationally faster. Combining the capabilities of ANN and GA is termed as Neuro-Genetic optimization. Madadi and Balaji [13] optimized the location of multiple discrete heat sources in a ventilated cavity using combined ANN and GA. ANN was trained using the data obtained from computational fluid dynamics, and the trained ANN was combined with a genetic algorithm for performing the optimization. Lee et al. [14] used the results of finite element analysis of micro-compact heat exchangers for training ANN, and later ANN was combined with GA for performing optimization. Neuro-Genetic optimization is found to be efficient in terms of computational time and thus is selected for this study.

The partial fraction set of conjugate heat transfer simulations to be carried out for training ANN is obtained from Taguchi's orthogonal arrays. The orthogonal array supports the design process and significantly reduces the number of simulations, saving time and resources. Jaya Krishna [15] optimized the phase change material heat sink using the Taguchi method, followed by melt fraction and maximum base temperature analysis. Aly [16] used the Taguchi method for finding the optimum condition for the heat transfer design parameters of the coiled tube-in-tube heat exchanger under turbulent flow conditions. To observe the effect of specific geometric parameters of H-type finned tube heat exchangers, Wang et al. [17] used Taguchi's process. The effects of Reynold number, fin height, and pitch on the heat transfer efficiency of a heat exchanger having cylindrical pin fins positioned in a rectangular channel were experimentally studied using the Taguchi method by Sahin [18]. Altan [19] used the L_{27} orthogonal array to produce 21 training data and six test data for the shrinkage prediction algorithm of a back-propagation neural network. Taguchi orthogonal arrays possess considerable advantages in providing the partial fraction set of conjugate heat transfer analysis required to train ANN and are adopted in this study.

The present paper combined the advantages of three efficient methods in various phases of the optimization process, namely, Taguchi method for the design of experiments, the trained artificial neural network using conjugate heat transfer simulations, for estimating output parameters for a set of input variables, and the genetic algorithm for carrying out multi-parametric optimization. Combining the Taguchi method, ANN, and the GA for optimization studies of complicated problems is called Taguchi-Neuro-Genetic methodology.

Summarizing this section of the paper, the literature survey on space radiators indicates that a large portion of the literature available in the public domain deals with optimizing parallel radiator configuration for space applications. The motivation behind the present work is to analyze the performance of the serial radiator, which has proven advantages on the ground, for space applications and to arrive at an optimized serial radiator configuration. The specific objectives of the study are as follows:

(a) To propose and study the serial radiator configuration for space application.
(b) To analyze the effects of various geometric and flow parameters on the performance of an MPFL parallel/serial radiator through conjugate heat transfer simulations.
(c) To optimize the parallel and serial radiator configurations using Taguchi-Neuro-Genetic approach
(d) To bring out the superior radiator configuration for different optimization objectives
    (i) Case 1: the objective is to minimize the sum of nondimensional mass and pumping power for a given heat rejection
    (ii) Case 2: the objective is to minimize nondimensional mass for a given heat rejection
    (iii) Case 3: the objective is to minimize nondimensional pumping power for a given heat rejection.

2 Radiator Configurations and Inputs for the Analysis

2.1 Radiator Configurations. For the present study, radiators are envisaged as four flat panels arranged around the service module of a human space flight, as shown in Fig. 1. Two radiator configurations are considered for the study: (1) conventional parallel radiator and (2) proposed serial radiator.

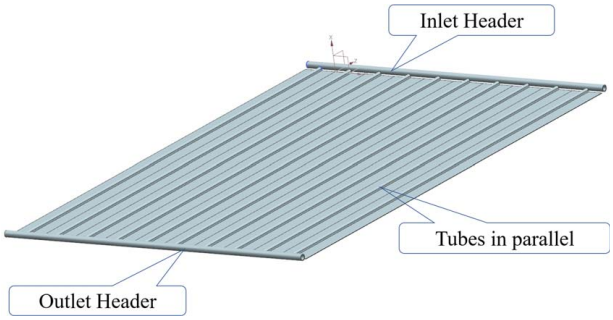

Fig. 2 Parallel radiator configuration

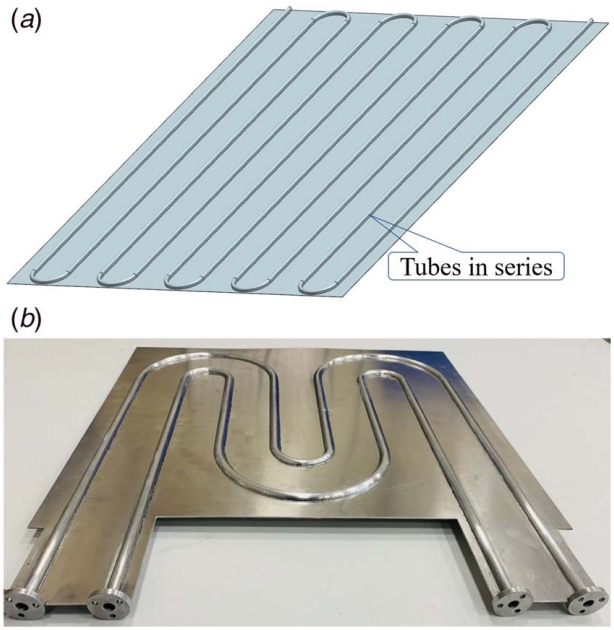

Fig. 3 Serial radiator panel configuration: (*a*) schematic and (*b*) realized radiator

2.1.1 Parallel Radiator Configuration. In the parallel radiator configuration, the tubes inside the radiator are arranged parallel to each other, as shown in Fig. 2. Flow is drawn to the tubes from a common inlet header and dumped into a common outlet header. As the radiators are segregated as four parallel independent panels, the flowrate to each radiator panel is 1/4th of the total flowrate of the external radiator loop of the thermal control system. With a pitch of 100 mm, a radiator panel of width 1 m consists of ten tubes in parallel. Thus, the coolant flowrate to each tube for this case is 1/40th of the total coolant flowrate.

2.1.2 Serial Radiator Configuration. In the serial radiator configuration, the tubes in the radiator panel are connected in serial. Thus, each radiator panel is considered to have one tube running all along the panel in a serpentine fashion, as shown in Fig. 3. The coolant flowrate to this tube is 1/4th of the total coolant flowrate of the ERL of TCS. Unlike parallel radiator configuration, serial radiator configuration does not require common inlet and outlet headers.

2.2 Parameters Influencing the Performance of a Radiator. The performance of the radiator is assessed through the following parameters:

(a) Heat rejection to space (Q) in Watts is given by Eq. (1)

$$Q = \sigma \varepsilon F A (T_{\text{rad}}^4 - T_{\text{sink}}^4) \tag{1}$$

(b) Total mass of the radiator (M) in kg is given by Eq. (2)

$$M = m_1 + m_2 + m_3 + m_4 + m_5 \tag{2}$$

(c) Specific heat rejection (SHR) in W/kg is given by Eq. (3)

$$SHR = Q/M \tag{3}$$

(d) Pumping power (Π) in Watts is given by Eq. (4)

$$\Pi = \frac{\text{Total Volume flow rate} \times \text{Total pressure drop}}{\text{Efficiency of pump}}$$

$$\Pi = \frac{(4 \times m_{\text{dot}}/\rho_f)(\Delta P + 15{,}000)}{\eta_p} \tag{4}$$

Since the pump has to circulate the coolant in the entire ERL and as four radiators are connected in parallel in ERL, the total mass flowrate in ERL is four times the m_{dot} per radiator. Apart from pressure loss in the radiator (ΔP), the pump in the ERL has to overcome the frictional losses, bend losses in the main plumb lines as well as pressure drop in components in the ERL such as interface heat exchanger, solenoid valves, check valves, and flow proportioning valve. The losses in main plumb lines and component losses are independent of the geometric configuration of the radiator tubes and thus considered as a constant value of 15,000 Pa. Thus, the total pressure loss that the pump has to overcome is ($\Delta P +$ 15,000) Pa. The overall efficiency of the pump (η_P) is considered as 30%.

For an ideal radiator, the heat rejection requirement shall be met with the minimum mass of the radiator and the pumping power requirement.

For a given external environment and radiator area, the parameters influencing the performance of the radiator, as depicted in Fig. 4, are as follows:

(i) *Geometric parameters*
  (a) Diameter of the tube running through the radiator panel (d_i)
  (b) Thickness of radiator fins (t_f)
  (c) Pitch of the tubes in radiator panel (P_i)
  (d) Thermo-optic properties of the radiating surface

(ii) *Flow parameters*
  (e) Fluid type and its properties
  (f) Mass flowrate of fluid passing through the tubes (m_{dot})
  (g) Temperature of fluid at the inlet of the radiator (T_{in})

(iii) *Fin and tube material properties*

For the present study, the thermo-optic surface properties of the radiator, fluid type, fluid inlet temperature to the radiator, fin and tube materials are frozen, keeping d_i, t_f, P_i, and m_{dot} as variables.

2.3 Material Selection. Aluminum alloy AA6061-T6 is selected as the fin and tube material for better weldability, brazeability, workability, and machinability. Strength and corrosion resistance are increased with tempering.

3M™ NOVEC™ 7100 is selected as the heat transfer fluid for its better thermophysical properties and lower freezing point. Table 1 gives the thermophysical properties of the selected materials.

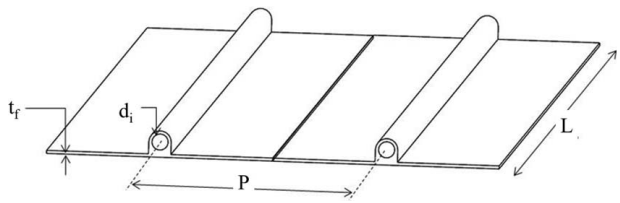

Fig. 4 Schematic of radiator showing variable parameters

Table 1 Thermophysical properties of selected materials

	AA6061-T6 [20]	3M™ NOVEC™ 7100 [21]
Density (ρ), kg/m^3	2700	1510
Conductivity (K), W/mK	160	0.069
Specific heat (C_p), J/kgK	896	1183
Dynamic viscosity (μ), Pas	–	5.8×10^{-4}
Freezing point, °C	–	−135

2.4 Inputs for the Analysis:. This study considered an orbit of about 400 km altitude and with an attitude of spacecraft such that there is no direct solar flux on the radiators. In such orbit, the albedo (Λ) is 239 W/m^2 and earthshine ($\ddot{E}$) is 200 W/m^2 [22].

Typically, the radiators are coated with white paint to increase the radiation emission to deep space and decrease external heat load absorption. Typical surface optical properties of white paint are solar absorptivity of 0.15 and IR emissivity of 0.9. Thus, the external heat load on radiators is given by Eq. (5)

$$q_{\text{ext}} = \alpha_s \times \Lambda + \varepsilon_{\text{IR}} \times \ddot{E}$$

$$q_{\text{ext}} = 0.15 \times 239 + 0.9 \times 200$$

$$\therefore q_{\text{ext}} = 216 \text{ W/m}^2 \quad (5)$$

While on the radiator toward the space side, the external heat load remains zero. Thus, an average external heat load on all four radiators will be in the order of 100 W/m^{2,} and this value is considered for the present study.

The external heat load and the ambient space temperature are converted to equivalent sink temperature through Eq. (6) [23]

$$T_{\text{sink}} = T_{\text{space}} + \left(q_{\text{ext}}/F\sigma\varepsilon\right)^{1/4} \quad (6)$$

3 Methodology

The methodology adopted for optimization of radiators is Taguchi-Neuro-Genetic approach, which is depicted through a block diagram given in Fig. 5. The radiator performance is analyzed through the steady-state conjugate heat transfer simulations. The minimum partial fraction set of simulations to uniformly cover the entire design domain is obtained through Taguchi's orthogonal arrays. Conjugate heat transfer simulations are then carried out for the set obtained through Taguchi's orthogonal array. The data obtained from the conjugate heat transfer simulations is used to train the ANN, and the trained ANN is coupled with GA to optimize radiators. Detailed briefing of each process in the methodology is given below.

3.1 Conjugate Heat Transfer Simulations. The conjugate heat transfer simulations are carried out using the "Electronics System Cooling" module of Siemens' NX software. A fully coupled pressure–velocity solver with a mixing length turbulence model is used for the simulations. The fluid is modeled as 3D HEX elements with boundary layer mesh at the fluid–solid interface, and solid is modeled as 3D TET4 elements. Fluid mesh parameters are given as 0.5 mm element size with a surface maximum growth rate of 1.3 to obtain a wall $y+$ of 0.9. Figure 6 displays the mesh used for conjugate heat transfer simulations. The fluid and fin elements are provided with an advanced coupling option to ensure the convective heat transfer from fluid elements to neighboring fin elements.

In parallel radiator configuration, the coolant to all parallel tubes enters at the top and exits from the bottom. Thus, the significant temperature gradient on the radiator surface is longitudinal (top to bottom). In the lateral direction, about the centerline between two tubes, the temperature distribution is symmetrical. Hence, an adiabatic boundary condition can be considered at the centerline between the adjacent tubes. Thus, it is possible to treat the problem using the fact that the analysis of one set of finned-tubes can be extended for the whole radiator.

While in serial radiator configuration, the exit of one straight tube is connected to the inlet of the other straight tube through U-bent tubes. The temperature distribution about the centerline between the tubes in the lateral direction is not symmetrical. Thus, for serial radiator configuration, the entire panel has to be modeled for the simulation.

3.1.1 Assumptions

(i) Fin material is assumed to be isotropic.
(ii) The thermophysical properties of fin material and coolant are assumed to be constant within the temperature range of the problem.
(iii) Orbit average external heat load is used for estimating the average sink temperature.

3.1.2 Boundary Conditions

(i) Radiation from the flat surface of the radiator to sink temperature.
(ii) Adiabatic boundary condition is specified on all other external surfaces of the radiator.

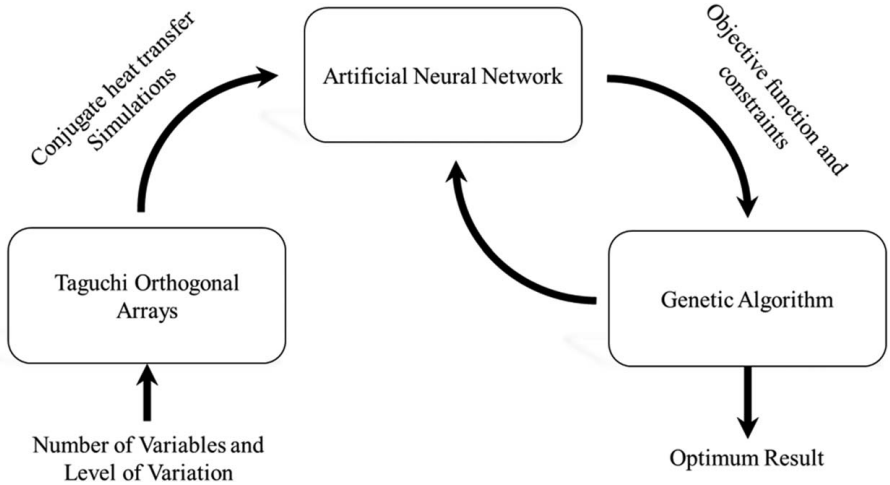

Fig. 5 Block diagram of Taguchi-Neuro-Genetic Approach

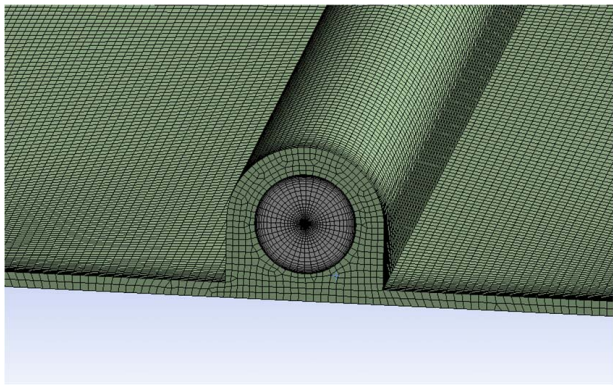

Fig. 6 Mesh with fluid and solid elements of radiator (gray color is fluid)

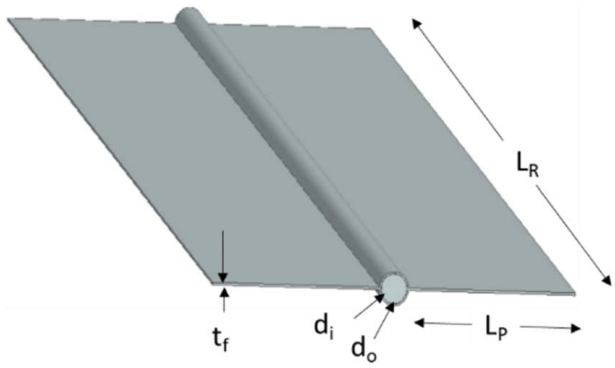

Fig. 7 Configuration chosen for validation studies

(iii) Coolant mass flowrate and inlet temperature are specified at the inlet of the tube.
(iv) Pressure outlet is specified at the outlet of the tube.
(v) Thermal coupling between fluid and fin elements.

3.1.3 Validation of Conjugate Heat Transfer Simulations. The baseline configuration for validating the conjugate heat transfer analysis is chosen from the work carried out by Kumar Rai et al. [5]. A radiator with 20 numbers parallel finned-tubes shown in Fig. 7 is modeled as per the dimensions given in Table 2. Kumar Rai et al. [5] provided the properties of materials to be used for comparative studies. External absorbed heat load (50 W/m^2) on the radiator is converted to sink temperature (182 K) as per the procedure provided in Sec. 2.4. Mass flowrate and inlet temperature of the fluid, as provided in Table 2, are chosen as input parameters.

Table 2 Input parameters of the validation case by Kumar Rai et al. [5]

Geometric parameters	
Fin thickness, t_f	0.6 mm
Inner diameter of the tube, d_i	7.5 mm
Outer diameter of the tube, d_o	8.5 mm
Length of fin, L_P	48.4 mm
Length of tube, L_R	475 mm
Thickness of tube, t_t	0.5 mm
Number of tubes, N_t	20
Input conditions	
Mass flowrate of coolant, m_{dot}	0.002 kg/s
Fluid inlet temperature, T_{in}	325 K
Emissivity of radiating surface, ϵ	0.8
Space ambient temperature, T_{space}	0 K
External absorbed heat load on top and bottom surfaces, q_{top} and q_{bot}	50 W/m^2
Sink temperature on top and bottom surfaces, T_{sink}	182 K

Table 3 Results of validation studies

	Validation case by Kumar Rai et al. [5]	Conjugate heat transfer analysis
Fluid outlet temperature, K	317.09	317.65
Mass of radiator, kg	2.265	2.2645
Heat rejection capacity, W/m^2	588.61	588.11

Table 3 compares the results of conjugate heat transfer simulations and the results reported by Kumar Rai et al. [5]. The surface plot of temperature is shown in Fig. 8. It is observed that the difference is less than 1%, and thus, the present methodology is validated.

3.2 Taguchi Orthogonal Arrays for Design of Experiments/Simulations. Ideally, a full factorial design will identify all possible combinations for a given set of factors. With number of variables as 4 and each variable has a level of variance of 5, the full factorial simulations would require $5^4 = 625$ runs. Conducting full factorial of 625 runs is computationally time consuming. To reduce the number of simulations to a practical level, Taguchi's orthogonal arrays for designing experiments (in this study these are simulations) are utilized. The columns of designed orthogonal arrays are balanced in two ways. First, the columns are balanced so that they have equal levels for each factor, i.e., the columns are balanced within themselves. Second, any two columns are balanced among themselves such that together an equal number of possible combinations are generated. Design of experiments involves the following steps:

(a) *Selection of independent variables:* The number of variables (n) in this study is 4; inner diameter and pitch of tubes in the radiator, thickness of radiator fin, and mass flowrate of coolant in the radiator
(b) *Selection of the number of level settings of each variable:* Each variable is varied at a level (l) of 5 to capture the nonlinear trend of the output parameters.
(c) *Selection of orthogonal array:* For selecting the orthogonal array, the minimum number of experiments to be conducted shall be fixed based on the degrees of freedom, which is given by Eq. (7)

$$N_{\text{Taguchi}} = 1 + \sum_{i=1}^{n} (l_i - 1) \tag{7}$$

From Eq. (7), N_{Taguchi} is 17 for $n = 4$ and $l = 5$. The orthogonal array shall be greater than the degrees of freedom and shall be second power of level of variance. Orthogonal array L_{25}, which

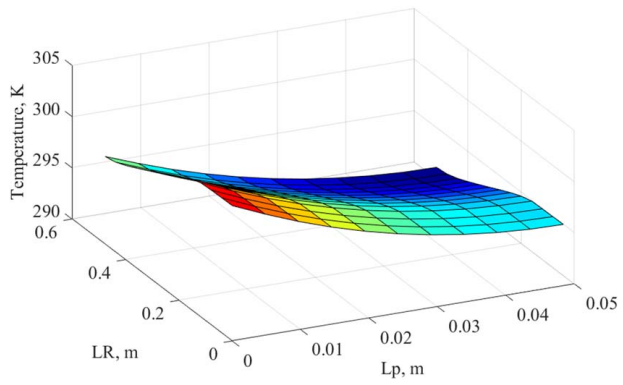

Fig. 8 Surface temperature plot for validation case

Table 4 Input variables and their levels

	Level 1	Level 2	Level 3	Level 4	Level 5
Diameter of the tube (d_i), mm	4	8	12	16	20
Thickness of fin (t_f), mm	0.6	0.8	1.2	1.4	1.6
Pitch of tubes (P_i), mm	20	60	100	140	180
Mass flowrate per radiator (m_{dot}), g/s	10	25	50	75	100

meets both the requirements is the right choice for this study. Table 4 provides the input variables and their levels and Table 5 provides the L_{25} orthogonal array. Columns of the Table 5 represent variables and the number in the orthogonal cell represents the level assigned to the variable. Each row represents the combination that serves as the simulation set. For instance, simulation no. 10 corresponds to $d_i = 8$ mm, $t_f = 1.6$ mm, $P_i = 20$ mm, and $m_{dot} = 25$ g/s.

3.3 Artificial Neural Network to Estimate Output Parameters for a Set of Input Variables. Artificial neural network is created through a standard Neural Net Fitting toolbox available in MATLAB® version R2020a. The conjugate heat transfer analysis data set is used for training the ANN. The ANN with input and output layers and one hidden layer, as shown in Fig. 9, is used in the present investigation. The number of neurons in the hidden layer is a tradeoff between the flexibility and overfitting of the network. Higher the number of neurons better will be the flexibility. With higher number of neurons, the total parameters (including weights, bias, etc.) in the network will be higher. Because of the fact that the total training data set shall be larger than the total parameters to avoid overfitting, the number of neurons shall be kept minimum. For the present study, where four input parameters and three output parameters exist, the number of neurons in hidden layer is selected as 4. The total number of parameters is 35 (Weights from the input layer to hidden layer: $4 \times 4 +$ bias on hidden neurons: $4 +$ weights from hidden layer to output layer: $4 \times 3 +$ bias on output parameters: 3). Thus, training data shall be greater than 35 cases, whereas the minimum set of simulations obtained from Taguchi's orthogonal array is only 25. Additional random simulation sets are conducted using conjugate heat transfer simulations and are used to train the ANN. In addition to increasing the number of simulations, the Bayesian regularization algorithm is used to avoid overfitting and increase the generalization of the network. All the input variables and output parameters are normalized between −1 and 1, and the hyperbolic tangent activation function is used at each neuron. About 85% of the conjugate heat transfer simulation data is used for training, and 15% is used for test.

The regression obtained for the network is close to 0.995, with a mean squared error of less than 0.001, indicating that the trained ANN predicts output very close to the target value for given input variables; the same can be observed from the plot given in Fig. 10, where the comparison is drawn between the heat rejected estimated by conjugate heat transfer analysis and that predicted by ANN. Trained ANN predicts the heat rejection within 1% of the value estimated by conjugate heat transfer analysis.

3.4 Genetic Algorithm for Multi-Parametric Optimization. The trained ANN is coupled with the GA to perform the multi-parametric optimization. Standard GA function in MATLAB® is used. The initial population of random chromosomes containing the input parameters, d_i, t_f, P_i, and m_{dot}, generated by GA, is fed to ANN to predict output parameters; total heat rejected, mass, and pumping power required. Based on the objective function, the fitness score is allocated to each chromosome. A cross-over operation between highly fit and inferior chromosomes is carried out, followed by a mutation operation, in which the genes of one of the individual chromosomes are mutated to form the new generation population. The new generation population is then fed to the trained ANN to obtain the objective function based on the out parameters. The iterative loop continues until the output parameters converge. The flowchart for the Taguchi-Neuro-Genetic optimization process is displayed in Fig. 11.

The optimization objective is to obtain a combination of input parameters that provide the lowest mass and lowest pumping power required for a given total heat rejection. For achieving this, a composite objective function, which is the sum of nondimensional mass and nondimensional pumping power, is used

$$\textit{Composite Objective function} = (M/M_o) \times w_1 + (\Pi/\Pi_o) \times w_2 \quad (8)$$

4 Results and Discussion

The performance of parallel and serial radiator configurations is independently assessed through the conjugate heat transfer simulations and compared. The baseline configurations for both parallel and serial configurations, as shown in Table 6 are selected to carry out the performance analysis. Apart from the simulation sets obtained through Taguchi's orthogonal arrays, nineteen other simulations were carried out, for each of parallel and serial radiators, by varying one of the parameters for each simulation with respect to the baseline configuration.

Figure 12 displays the comparison of parallel and serial radiator performance obtained by varying the tube inner diameter. For both the configurations, heat rejected by radiator decreases with an increase in tube diameter. This is because, for a given mass flowrate, with an increase in tube diameter, the velocity of flow in tube decreases, resulting in lower Reynolds number and eventually lower heat transfer coefficient from fluid to the fin surface. It is also observed that, for parallel radiator configuration, the increase in tube diameter beyond $d_i/d_{i,o}$ of 0.4 has an insignificant effect on the heat rejection because of the fact that at $d_i/d_{i,o}$ of 0.4 and beyond, the flow in the tube remains in the laminar regime. Reynolds number for a tube diameter $d_i/d_{i,o}$ of 0.2 is 2745 (transition regime), while for a tube diameter $d_i/d_{i,o}$ of 0.4 is 1373 (laminar regime). It is also evident that the mass of the radiator increases with the increase in tube diameter for both the configurations. The findings on the variation of heat rejection and the radiator mass with tube diameter agree with the study reported by Afshari et al. [2]. The increase in the mass of parallel radiator is steeper compared with that of the serial radiator due to the increase in header mass of parallel radiator at a higher tube diameter. Figure 13 displays the comparison of SHR of parallel and serial radiators with variation in tube diameter. SHR is defined as the ratio of total heat rejection to the total mass of the radiator. A decrease in heat rejection and increase in mass leads to a decrease in SHR with increased tube diameter for both parallel and serial radiators. It can be noted that, at any tube diameter, the SHR of the serial radiator is higher than the parallel radiator indicating the serial radiator is a better thermal performer than the parallel radiator.

Figure 14 displays the comparison of parallel and serial radiator performance with varying fin thickness (t_f). With an increase in fin thickness, a gradual increase in heat rejection is observed for the both configurations. The cross-sectional area available for heat conduction increases with fin thickness, leading to a higher average fin temperature. The fin tip temperature will be closer to the fin base temperature for higher fin thickness, leading to higher radiator efficiency. The mass of both the radiator configurations increases

Table 5 Standard L_{25} orthogonal array

Simulation no.	Diameter of tube, d_i	Thickness of fin, t_f	Pitch of tubes, P_i	Mass flowrate per radiator, m_{dot}
1	1	1	1	1
2	1	2	2	2
3	1	3	3	3
4	1	4	4	4
5	1	5	5	5
6	2	1	2	3
7	2	2	3	4
8	2	3	4	5
9	2	4	5	1
10	2	5	1	2
11	3	1	3	5
12	3	2	4	1
13	3	3	5	2
14	3	4	1	3
15	3	5	2	4
16	4	1	4	2
17	4	2	5	3
18	4	3	1	4
19	4	4	2	5
20	4	5	3	1
21	5	1	5	4
22	5	2	1	5
23	5	3	2	1
24	5	4	3	2
25	5	5	4	3

linearly with an increase in fin thickness. Figure 15 displays the comparison of SHR of parallel and serial radiator with variation in fin thickness. The increase in mass dominates the increase in heat rejection, leading to a decrease in SHR with an increase in fin thickness for both parallel and serial radiators. It can be noted that the SHR of the serial radiator is higher than the parallel radiator at any fin thickness.

Figure 16 displays the comparison of parallel and serial radiator performance with varying pitch of tubes (P_i). With an increase in pitch, the heat rejection by both the configurations reduces. At the pitch value ($P_i/P_{i,o}$) of 0.11, the heat rejected by the parallel and serial radiator configurations is of the same order because, at very low pitch, the significant portion of the radiator area is covered with the tube base resulting in better heat rejection to space and thereby, the insignificant difference exists between heat rejection by parallel and serial radiators. The lower the pitch, the closer is the fin tip temperature to that of the fin base. Hence, low pitch leads to higher heat rejection capacity and higher efficiency of the radiator. As the pitch of the tubes increases, the reduction in heat rejected for the parallel radiator is steeper than that of the serial

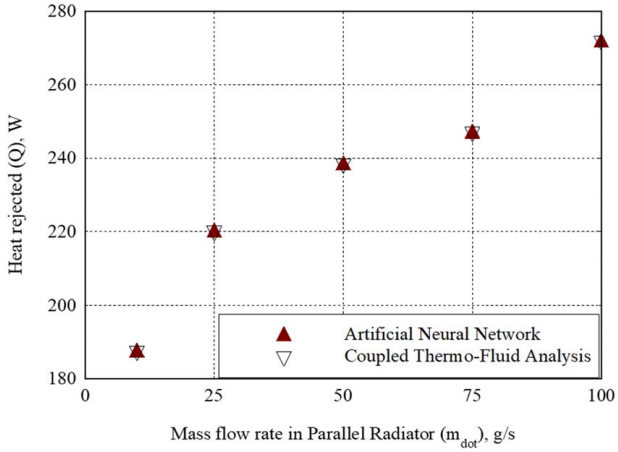

Fig. 10 Comparison of results between conjugate heat transfer analysis and trained ANN

radiator. Mass of both the radiator configurations reduces with an increase in the pitch of tubes. Figure 17 displays the comparison of SHR of parallel and serial radiators with variation in pitch of the tubes. At smaller pitch of the tubes, up to $P_i/P_{i,o}$ of 0.55, with increase in pitch of tubes, the decrease in mass is prominent than the decrease in heat rejection, leading to a higher SHR for both parallel and serial radiators. At higher pitch of the tubes, above $P_i/P_{i,o}$ of 0.77, the decrease in heat rejection is compensated by the decrease in mass, leaving SHR almost unchanged with the increase in pitch of tubes. At any pitch of tubes, it can be noted that the SHR of serial radiator is higher than the parallel radiator.

A comparison between parallel and serial radiator performance with change in the coolant mass flowrate is displayed in Fig. 18. A higher mass flowrate leads to a higher velocity of flow inside the tube, resulting in a higher Reynolds number and higher heat transfer between the flow and the fin surface. It is observed that the profile of the heat rejection curve for parallel radiator changes at a mass flowrate ($m_{dot}/m_{dot,o}$) of 0.75, because the flow inside the tube transits to turbulent regime above ($m_{dot}/m_{dot,o}$) of 0.75. The increase in the pressure drop with increase in the mass flowrate results in a higher pumping power requirement for both configurations. Flow transition from laminar to turbulent regime occurs for the parallel radiator configuration, whereas the flow for the entire range of flowrates of the present investigation remains in the turbulent regime for serial radiator configuration. For the coolant mass flowrates under consideration, the heat rejected and pumping power required by the serial radiator are higher than those of parallel radiator.

Serial radiator provides higher heat rejection at lower mass but requires higher pumping power for a given geometric and flow parameters, than parallel radiator configuration. However, a detailed

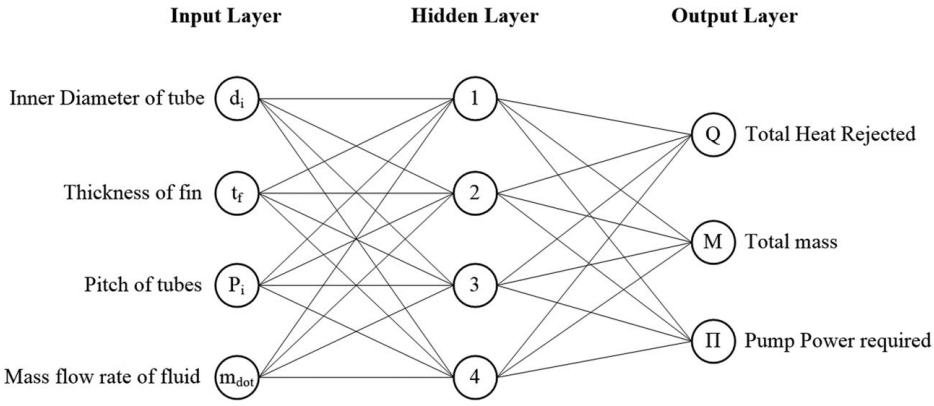

Fig. 9 Artificial neural network architecture

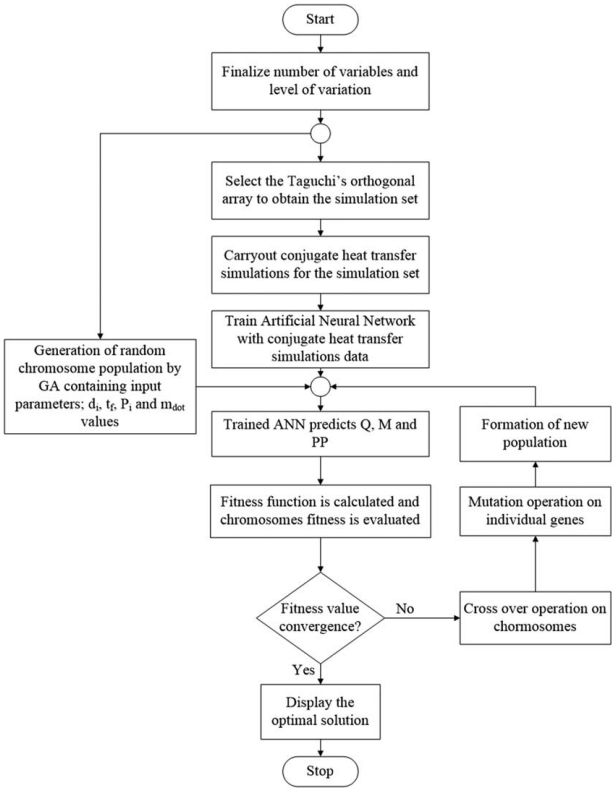

Fig. 11 Flowchart of optimization through Taguchi-Neuro-Genetic approach

Table 6 Baseline configuration used for parallel and serials radiator configurations

	Parallel	Serial
Geometric parameters		
Tube internal diameter (d_i), mm	8.0	8.0
Length of the radiator (L), m	1.5	1.5
Width of the radiator, m	1.0	1.0
Fin thickness (t_f), mm	1.2	1.2
Pitch of tubes, mm	100.0	100.0
Flow parameters		
Mass flowrate of the fluid in the radiator (m_{dot}), g/s	50.0	50.0
Temperature of coolant at the inlet of the tube (T_{in}), K	283	283

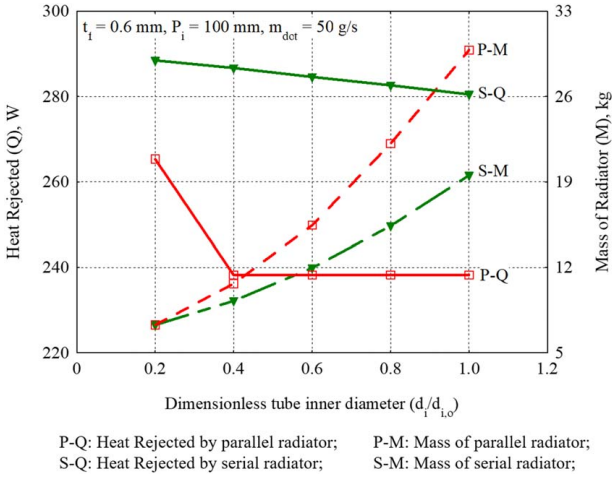

Fig. 12 Comparison of performance of parallel and serial radiators with variation in tube diameter

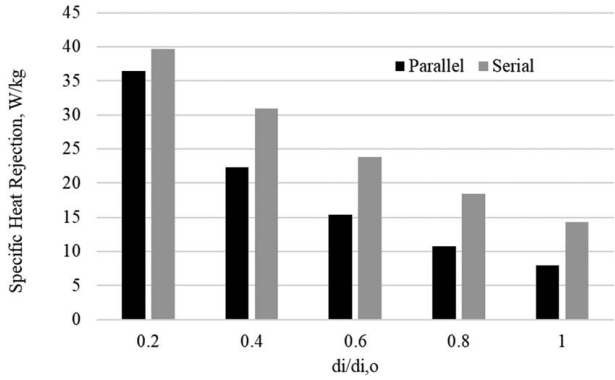

Fig. 13 Comparison of specific heat rejection of parallel and serial radiators with variation in tube diameter

comparison between the two configurations for optimum geometric and flow parameters for given heat rejection is addressed in Sec. 4.1.

4.1 Optimization and Comparison of Optimum Radiator Configurations. The Taguchi-Neuro-Genetic approach was applied for both parallel and serial radiator configurations. The objective function chosen is the composite objective function, which is the sum of nondimensional mass and nondimensional pumping power with weighing factors as given in Eq. (8), with equality constraint imposed on the total heat rejection. In addition to the equality constraint on total heat rejection, inequality constraints on the Pitch of the tubes based on the fabrication aspects were also considered. The minimum bend radius of Aluminum tubes shall be greater than three times the outer diameter of the tube [24]. Considering this aspect, a constraint is posed on the pitch of tubes in serial radiator configuration. In parallel radiator configuration, the tubes have to be welded to the inlet and outlet headers, for which a minimum clearance of 30 mm between the tubes is required. Accordingly, the pitch of the tubes in parallel radiator configuration are constrained.

Three different cases were considered for optimization study. For case 1, equal weightage is given for both mass and pumping power by choosing w_1 and w_2 as 1. For case 2, full weightage is given to mass by choosing $w_1 = 1$ and $w_2 = 0$. For case 3, full weightage is given to pumping power by choosing $w_1 = 0$ and $w_2 = 1$.

Tables 7 and 8 provide the input parameters and the results of optimization, respectively. For case 1, where equal weightage is given to minimize both mass and pumping power, the optimum

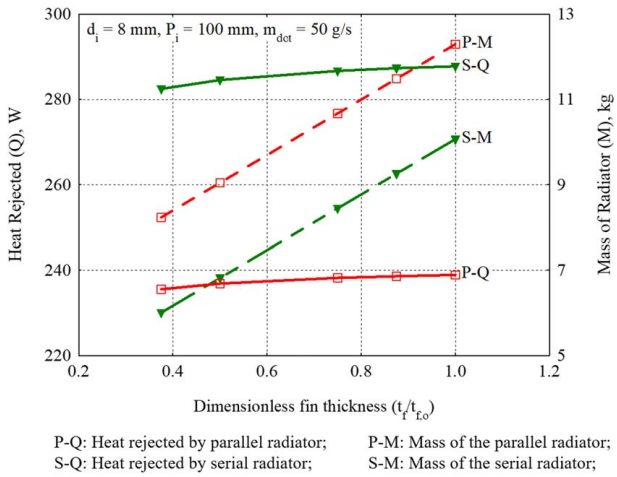

Fig. 14 Comparison of performance of parallel and serials radiators with variation in fin thickness

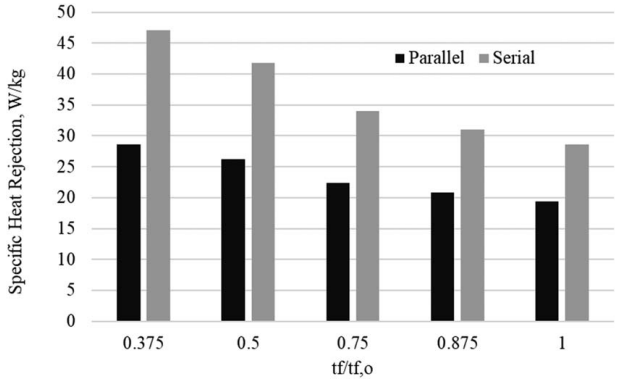

Fig. 15 Comparison of specific heat rejection of parallel and serials radiators with variation in fin thickness

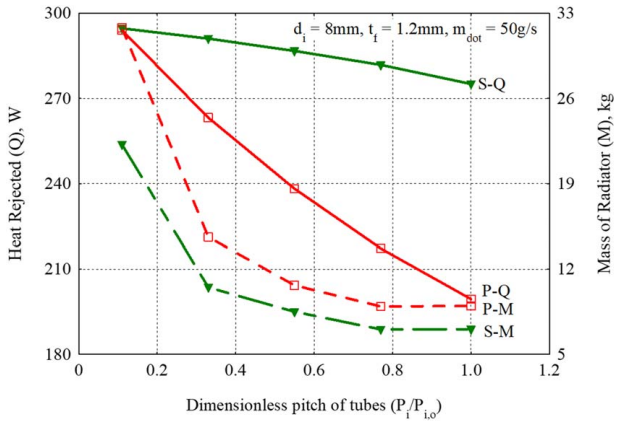

Fig. 16 Comparison of performance of parallel and serial radiators for varying pitch of tubes

parallel radiator is about 20% heavier and requires about 35% more pumping power than the optimum serial radiator. As the objective of the optimization is to minimize the composite objective function, the value of composite objective function, which is about 27% higher for parallel radiator than the serial radiator, indicates that the serial radiator is a better performer.

For case 2, where total weightage is given to minimize the mass of the radiator, the optimum parallel radiator is about 102% heavier than the optimum serial radiator. For case 3, where total weightage

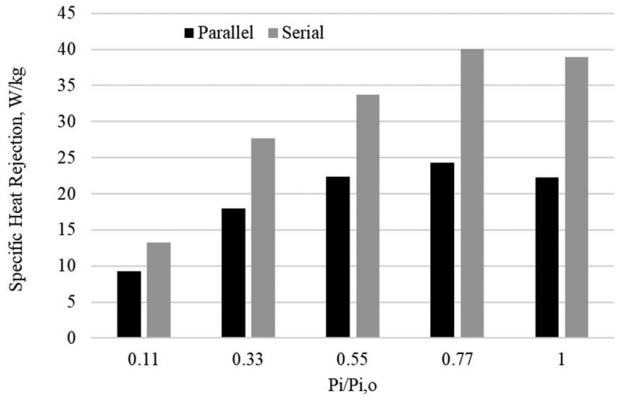

Fig. 17 Comparison of specific heat rejection of parallel and serial radiators with variation in pitch of tubes

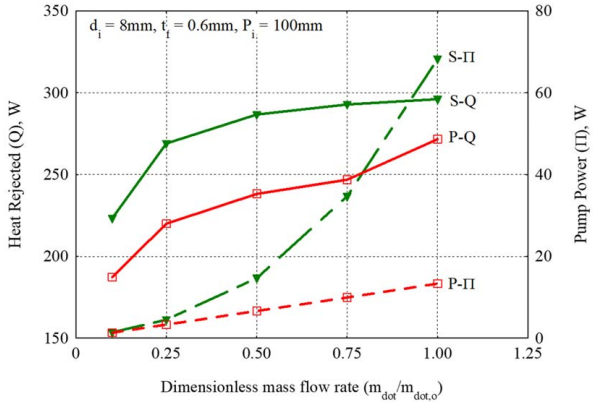

Fig. 18 Comparison of performance of the parallel and serial radiators for varying pitch of tubes

Table 7 Input parameters for optimization

Total heat rejected	270 W
Area of radiator	1.5×1 m^2
Fluid inlet temperature, T_{in}	283 K

is given to minimize the pumping power requirement of the radiator, the optimum parallel radiator requires about 64% higher pumping power than the optimum serial radiator.

For all three optimization cases, the serial radiator displays superior performance in terms of lower mass and lower pumping power requirement for a given heat rejection than the parallel radiator. From the performance analysis, it was observed that at any mass flowrate, serial radiator requires higher pumping power than the parallel radiator. However, from the optimization study, it is clear that for a given heat rejection, mass flowrate requirement of serial radiator is lesser than the parallel radiator, causing the serial radiator to consume less pumping power than the parallel radiator.

The optimum configurations obtained from the Taguchi-Neuro-Genetic approach are analyzed through conjugate heat transfer simulations to verify the output. It was observed that there is a good match between the values of heat rejection, mass, and pumping power requirement obtained from the conjugate heat transfer simulations and those predicted by ANN.

Table 8 Optimization results

	Case 1: $w_1 = 1$; $w_2 = 1$		Case 2: $w_1 = 1$; $w_2 = 0$		Case 3: $w_1 = 0$; $w_2 = 1$	
	Parallel	Serial	Parallel	Serial	Parallel	Serial
Inner diameters (d_i), mm	4	8.7	4	4.0	4.0	8.7
Fin thickness (t_f), mm	1.2	0.6	1.4	0.6	1.6	1.6
Pitch of tubes (P_i), mm	102.5	108.0	135	180.0	30.0	108.0
Mass flowrate in radiator (m_{dot}), g/s	50	32	100	70.0	55.0	27
Total mass of radiator (M), kg	7.72	6.45	7.27	3.59	14.36	10.11
Pumping power (Π), W	7.64	5.67	17.97	340.30	7.34	4.47
Value of objective function	15.36	12.12	7.27	3.59	7.34	4.47

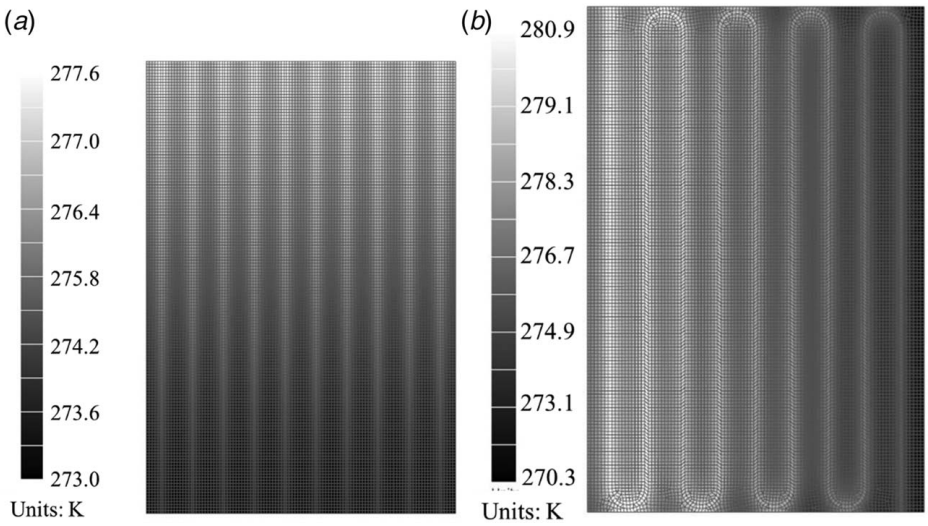

Fig. 19 Temperature palettes of optimum radiator configurations: (*a*) parallel radiator and (*b*) serial radiator

Figures 19(*a*) and 19(*b*) display the temperature palette obtained from conjugate heat transfer simulations for optimum parallel and serial radiator configurations, respectively. The hottest zone in the parallel radiator is at the top of the radiator, and the coldest zone is at the bottom of the radiator. The significant temperature gradient is along the tube length, from top to bottom of the radiator, compared with the gradient along the fin length. In contrast, the temperature gradient is along the width of the radiator in serial radiator configuration because of the fact that the flow enters at the left edge, travels all along the radiator flow path and exits at the right edge.

5 Conclusions

A serial radiator configuration, which has proven advantages in the ground applications, is proposed and analyzed for space applications. Parallel radiator configuration, which is well studied in the literature, is taken as a baseline configuration for comparing the performance of serial radiator configuration. Conjugate heat transfer simulations were performed by varying one variable parameter at a time to carry out performance analysis. From the performance analysis, it was observed that the specific heat rejection capacity, which is a ratio of total heat rejection to the mass of radiator, is higher for the proposed serial radiator than the conventional parallel radiator for any tube diameter, the thickness of fin and pitch of the tubes under consideration. The pumping power required by the serial radiator is higher than the parallel radiator for any mass flowrate under consideration. However, the total heat rejection is lower for parallel radiator than serial radiator for any mass flowrate. Thus, optimization of radiators is carried out by constraining the total heat rejection.

The Taguchi-Neuro-Genetic approach is adopted for performing design optimization. The conjugate heat transfer simulations were carried out for the partial factorial set of simulations determined by Taguchi's orthogonal arrays, covering the entire design domain. The simulation results were used to train ANN. The trained ANN predicts the output with an error of less than 1%. The trained ANN was coupled with the genetic algorithm to carry out multi-parametric optimization of radiator configurations. Through the Taguchi-Neuro-Genetic approach, the optimum parallel and serial radiator configurations are obtained. Optimization is conducted for three different cases. For case 1, where equal weightage is given to minimize both mass and pumping power for given heat rejection, the optimum parallel radiator is about 20% heavier and requires about 35% more pumping power than the optimum serial radiator. For case 2, where total weightage is given to minimize the mass of the radiator for given heat rejection, the optimum parallel radiator is about 102% heavier than the optimum serial radiator. For case 3, where total weightage is given to minimize the pumping power requirement of the radiator for given heat rejection, the optimum parallel radiator requires about 64% higher pumping power than the optimum serial radiator. From the results of case 1 and case 3, when an equality constraint is posed on total heat rejection, the pumping power requirement of the serial radiator is lower than the parallel radiator because the serial radiator requires a lower mass flowrate than the parallel radiator to reject a given heat load. From all three optimization cases, the proposed serial radiator turns out to be a superior performer in terms of lower mass and lower pumping power requirement than the conventional parallel radiator. Thus, it is concluded that for the spaceflights, where mass and power are of prime importance, the proposed serial radiator configuration has proven advantageous over conventional parallel radiator configuration. The serial radiator configuration and the optimization study results presented in this study can be applied to radiator design for human space flights and high-power satellites.

Acknowledgment

The authors would like to acknowledge the support provided by Shri K. G. Vinod and Shri Rajesha in providing the technical inputs and Shri Priyesh Kumar Jain, Ms. Samridhi Sharma, and Shri Dhanraj for providing support throughout the course of this work.

Conflict of Interest

There are no conflicts of interest.

Data Availability Statement

The datasets generated and supporting the findings of this article are obtainable from the corresponding author upon reasonable request. The authors attest that all data for this study are included in the paper.

Nomenclature

h = heat transfer coefficient
n = number of variables
A = area of radiator exposed surface
F = view factor from the surface to deep space
L = length of the radiator
M = total mass of the radiator including metal and fluid masses per unit area
Q = heat rejected by the radiator in Watts
$\ddot{\text{E}}$ = Earth Shine
d_i = inner diameter of the tube in the radiator
$d_{i,o}$ = diameter of tube used for nondimensionalization
l_i = level of variance of ith variable
m_{dot} = mass flowrate of coolant in radiator
$m_{\text{dot},o}$ = mass flowrate used for nondimensionalization
m_1 = mass of the radiator panel
m_2 = mass of tubes in the radiator
m_3 = mass of fluid in the tubes
m_4 = mass of header tube (only for parallel radiator configuration)
m_5 = mass of the fluid in header tubes (only for parallel configuration)
q_{ext} = external heat load on radiator (W/m^2)
t_f = thickness of radiator fin
$t_{f,o}$ = thickness of fin used for nondimensionalization
w_1 = weighing factor for mass
w_2 = weighing factor for pumping power
C_p = specific heat of the coolant/fin material
M_o = mass of radiator used for nondimensionalization, 1 kg
N_{Taguchi} = minimum number of simulations to be conducted based on Taguchi method
P_i = pitch of the tubes in radiator
$P_{i,o}$ = pitch of the tubes used for nondimensionalization
T_f = average fluid temperature in the tube
T_{in} = temperature of coolant at the inlet of the tube
T_{rad} = average surface temperature of radiator
T_{sink} = sink temperature
T_{space} = deep space temperature
α_s = solar absorptivity of the exposed surface of radiator
ΔP = pressure drop in the entire ERL
ε = IR emissivity of the radiating surface
η = efficiency of the radiator
η_P = efficiency of the pump
Λ = Albedo
Π or PP = pumping power
Π_o = pumping power used for nondimensionalization, 1 W
ρ_f = density of fluid
ρ_M = density of radiator tube and fin material
σ = Stefan Boltzmann constant

References

[1] Naumann, R. J., 2004, "Optimizing the Design of Space Radiators," Int. J. Thermophys., **25**(6), pp. 1929–1941.
[2] Afshari, B. M., Abedi, M., and Shahryari, M., 2017, "Optimization of a Radiator for a MPFL System in a GEO Satellite," Adv. Aircr. Spacecr. Sci., **4**(6), pp. 701–709.
[3] Salem, T. K., Nazzal, I. T., Arik, M., and Budakli, M., 2019, "Impact of Functional Nanofluid Coolant on Radiator Performance," ASME J. Therm. Sci. Eng. Appl., **11**(4), p. 041020.
[4] Võsa, K.-V., Ferrantelli, A., Kull, T. M., and Kurnitski, J., 2018, "Experimental Analysis of Emission Efficiency of Parallel and Serial Connected Radiators in EN442 Test Chamber," Appl. Therm. Eng., **132**, pp. 531–544.
[5] Kumar Rai, P., Rao Chikkala, S., Adoni, A. A., and Kumar, D., 2015, "Space Radiator Optimization for Single-Phase Mechanical Pumped Fluid Loop," ASME J. Therm. Sci. Eng. Appl., **7**(4), p. 041021.
[6] Deka, A., and Datta, D., 2017, "Geometric Size Optimization of Annular Step Fin Using Multi-Objective Genetic Algorithm," ASME J. Therm. Sci. Eng. Appl., **9**(2), p. 021013.
[7] Selleri, T., Najafi, B., Rinaldi, F., and Colombo, G., 2013, "Mathematical Modeling and Multi-Objective Optimization of a Mini-Channel Heat Exchanger Via Genetic Algorithm," ASME J. Therm. Sci. Eng. Appl., **5**(3), p. 031013.
[8] Dias, T., and Milanez, L. F., 2006, "Optimal Location of Heat Sources on a Vertical Wall With Natural Convection Through Genetic Algorithms," Int. J. Heat Mass Transfer, **49**(13–14), pp. 2090–2096.
[9] da Silva, A. K., Lorente, S., and Bejan, A., 2004, "Optimal Distribution of Discrete Heat Sources on a Wall With Natural Convection," Int. J. Heat Mass Transfer, **47**(2), pp. 203–214.
[10] Leong, C. H., Azid, I. A., and Seetharamu, K. N., 2002, "Thermal Performance Prediction of Plastics Ball Grid Array (PBGA) Using Artificial Neural Network," ASEAN J. Sci. Technol. Develop., **19**(1), pp. 29–38.
[11] Asok, S. P., Sankaranarayanasamy, K., Sundararajan, T., Rajesh, K., and Sankar Ganeshan, G., 2007, "Neural Network and CFD Based Optimization of Square Cavity and Curved Cavity Static Labyrinth Seals," Tribol. Int., **40**(7), pp. 1204–1216.
[12] Khan, T. A., and Li, W., 2018, "Optimal Configuration of Vortex Generator for Heat Transfer Enhancement in a Plate-Fin Channel," ASME J. Therm. Sci. Eng. Appl., **10**(2), p. 021013.
[13] Madadi, R. R., and Balaji, C., 2008, "Optimization of the Location of Multiple Discrete Heat Sources in a Ventilated Cavity Using Artificial Neural Networks and Micro Genetic Algorithm," Int. J. Heat Mass Transfer, **51**(9–10), pp. 2299–2312.
[14] Lee, H. W., Teng, Y. J., Azid, I. A., and Seetharamu, K. N., 2007, "Neuro-Genetic Optimization of Micro Compact Heat Exchanger," Int. J. Numer. Methods Heat Fluid Flow, **17**(1), pp. 20–33.
[15] Jaya Krishna, D., 2018, "Operational Time and Melt Fraction Based Optimization of a Phase Change Material Longitudinal Fin Heat Sink," ASME J. Therm. Sci. Eng. Appl., **10**(6), p. 064502.
[16] Aly, W. I. A., 2014, "Computational Fluid Dynamics and Optimization of Flow and Heat Transfer in Coiled Tube-in-Tube Heat Exchangers Under Turbulent Flow Conditions," ASME J. Therm. Sci. Eng. Appl., **6**(3), p. 031001.
[17] Wang, H., Liu, Y., Yang, P., Wu, R., and He, Y., 2006, "Parametric Study and Optimization of H-Type Finned Tube Heat Exchangers Using Taguchi Method," Appl. Therm. Eng., **103**, pp. 128–138.
[18] Sahin, B., 2007, "Taguchi Approach for Determination of Optimum Design Parameters for a Heat Exchanger Having Circular Cross-Sectional Pin Fins," Heat Mass Transfer, **43**, pp. 493–502.
[19] Altan, M., 2010, "Reducing Shrinkage in Injection Moldings via the Taguchi, ANOVA and Neural Network Methods," Mater. Des., **31**(1), pp. 599–604.
[20] ASM International, 1992, *ASM Handbook. Nonferrous Alloys and Special-Purpose Materials Volume 2, Metals Handbook*, ASM International, Materials Park, OH.
[21] 3M™ Novec™ 7100 Engineered Fluid Product Information, 2009, St. Paul, MN, https://multimedia.3m.com/mws/media/199818O/3m-novec-7100-engineered-fluid.pdf
[22] Gilmore, D., 2002, *Spacecraft Thermal Control Handbook, Volume 1: Fundamental Technologies*, American Institute of Aeronautics and Astronautics, Washington, DC. 10.2514/4.989117
[23] Çengel, Y. A., and Ghajar, A. J., 2011, *Heat and Mass Transfer: Fundamentals & Applications*, 2nd ed., McGraw-Hill, New York.
[24] "Tube Bend Radii," SAE AS33611, 2015, G-3, Aerospace Couplings, Fittings, Hose, Tubing Assemblies. 10.4271/AS33611.